
Article:
Conte, M. and Hippler, M. (2016) Dynamic NMR and Quantum-Chemical Study of the Stereochemistry and Stability of the Chiral MoO2(acac)2 Complex in Solution. J Phys Chem A. ISSN 1089-5639

https://doi.org/10.1021/acs.jpca.6b03563

Dynamic-NMR and Quantum-Chemical Study of the Stereochemistry and Stability of the Chiral $MoO_2(acac)_2$ Complex in Solution

Marco Conte * and Michael Hippler *

Department of Chemistry, University of Sheffield, Sheffield S3 7HF, United Kingdom
E-mails: m.conte@sheffield.ac.uk, m.hippler@sheffield.ac.uk.
MC: Telephone: +44 (0)114 222 9506
MH: Telephone: +44 (0)114 222 9505

Journal of Physical Chemistry A, DOI: 10.1021/acs.jpca.6b03563
Author accepted manuscript, 11-Aug-2016

ABSTRACT

The stereochemistry and dynamics of $MoO_2(acac)_2$ in benzene, chloroform and toluene was investigated by variable temperature ^{1}H NMR, density functional theory (SOGGA11-X, B3LYP) and *ab initio* (MP2) methods. In solution, an equilibrium between two chiral enantiomers with C_2 symmetry was identified, Λ-*cis*-$MoO_2(acac)_2$ and Δ-*cis*-$MoO_2(acac)_2$. The two enantiomers are connected *via* achiral *cis* transition states that switch the enantiomeric conformations *via* a Ray-Dutt, Bailar and a newly described racemization twisting mechanism. All three mechanisms have similar calculated activation energies. Activation parameters E_a, $\Delta H^{\ddagger}$, and $\Delta S^{\ddagger}$ were experimentally determined for the exchange process, with a small, negative $\Delta S^{\ddagger}$, and a positive $\Delta H^{\ddagger}$ of 68.1 kJ mol^{-1} in benzene, 54.9 kJ mol^{-1} in chloroform, and 60.6 kJ mol^{-1} in toluene, in reasonable general agreement with the calculations. *trans* configurations of $MoO_2(acac)_2$ are very much higher in energy than *cis* and are not relevant in the temperature range experimentally studied, 243-340 K. The enantiomers interconvert within seconds near room temperature, and much faster at elevated temperatures. Racemization will thus prevent the use of enantiomerically pure $MoO_2(acac)_2$ for chiral catalysis under practical conditions.

1. INTRODUCTION

$MoO_2(acac)_2$ is a well-known complex in inorganic chemistry,[1,2] which is mainly used as a precursor for the synthesis of molybdenum dioxo complexes $MoO_2(L)(X)$ where L is often a nitrogen ligand[3] and X a solvent molecule like water or an alcohol.[4] It also finds applications in catalysis for the epoxidation of alkenes[5] in a variety of forms, for example in solution and in presence of oxygen donors like *tert*-butyl hydro peroxide (TBHP), it is effective for the epoxidation of 1-octene,[6] squalene,[7] and cyclohexene.[8] It can also be used as immobilized species, either polymer bound[9] or over mesoporous silicates like MCM-41,[10] for the epoxidation of cyclohexene and cyclooctane. $MoO_2(acac)_2$ is also a precursor for heterogeneous Mo catalysts supported on Al_2O_3 and SiO_2 for metathesis reactions.[11] Among these applications in catalysis, one of particular interest is the chiral epoxidation of alkenes.[12] Using $MoO_2(acac)_2$ as a precursor this is usually achieved by substituting one of the acac ligands with a chiral ligand like alkoxo-imino species.[13] $MoO_2(acac)_2$ has the interesting property to exist as two chiral enantiomers in the solid state, Λ-*cis*-$MoO_2(acac)_2$ and Δ-*cis*-$MoO_2(acac)_2$ (see Fig. 1), which in principle could lead to chiral oxidation reactions. However, while the structural features of this complex are well established in the solid state,[14,15] little is known about the stereochemistry of this complex in solution,[16,17] where most epoxidation reactions are carried out. In fact, $MoO_2(acac)_2$ in solution is not capable to lead to any evident enantiomeric excess for epoxidation, unless chiral ligands are used.[18,19]

Moreover, despite frequent depictions of $MoO_2(acac)_2$ as *trans* species with D_{2h} symmetry in modern literature,[20-22] *trans*-$MoO_2(acac)_2$ does not exist in the solid state,[23] and its existence in the liquid phase has never been confirmed to the best of our knowledge. As the reactions mentioned above all occur in liquid phase, this prompted us to consider the actual stereochemistry of $MoO_2(acac)_2$ in solution.

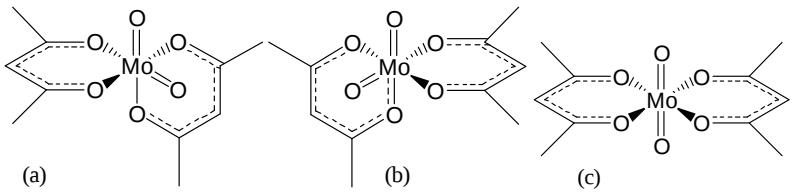

Figure 1. Molecular structures of **(a)** Λ-*cis*-$MoO_2(acac)_2$, **(b)** Δ-*cis*-$MoO_2(acac)_2$ and **(c)** *trans*-$MoO_2(acac)_2$. The chiral enantiomers have C_2 symmetry. D_{2h} symmetry is commonly assumed for *trans*-$MoO_2(acac)_2$ (see also discussion in main text).

In 1971, Craven *et al.* observed the existence of an equilibrium involving the *cis* species by analysis of variable temperature ^{1}H NMR data (60 MHz) of $MoO_2(acac)_2$ solutions in benzene and chloroform.[17] Coalescence of the ^{1}H NMR signal from the two non-equivalent methyl groups of the acac ligand was detected by increasing the temperature. The coalescence was tentatively explained by either rapid methyl migration between non-equivalent sites of the acac ligand or rapid equilibration of the *cis* isomers to form a *trans* isomer, as the latter has magnetically equivalent methyl groups. However, the *trans* isomer has not been observed so far.

With modern advances in NMR spectroscopy and computational tools, these open questions prompted us to re-investigate the stereochemistry and dynamic equilibrium of $MoO_2(acac)_2$ in solution with the aim to determine rate constants and thermodynamic activation parameters with a higher level of accuracy, and to identify possible structures of intermediates or transition states involved in this process. In fact, if enantiomer pure $MoO_2(acac)_2$ could be isolated and stabilized, this complex could provide an attractive route for chiral epoxidation reactions, and thus provide useful insights for future catalyst design.

2. EXPERIMENTAL AND COMPUTATIONAL METHODS

2.1 Variable temperature ^{1}H NMR.

Bis-acetylacetonate-dioxomolybdenum(VI) (Mo assay 26.5 - 33.2 wt %, here abbreviated as $MoO_2(acac)_2$), chloroform $CDCl_3$ (99.8% D), benzene C_6D_6 (99.6% D), and acetonitrile CH_3CN were purchased from Sigma−Aldrich and used as received. An additional set of experiments was carried out with $MoO_2(acac)_2$ purified by sublimation and anhydrous toluene-D_8 (C_7D_8, Sigma-Aldrich, 99% D). Toluene was dried using molecular sieves for 72 h using the protocol by Williams and Lawton[24] and references therein. $MoO_2(acac)_2$ solutions in $CDCl_3$, C_6D_6, and C_7D_8 (10^{-2} M) were prepared in a Norell 5 mm intermediate pressure valved NMR sample tube and sealed under atmospheric pressure at room temperature to prevent solvent escaping at elevated temperatures. Variable temperature ^{1}H NMR spectra of $MoO_2(acac)_2$ solutions were recorded at 500 MHz using a Bruker Avance III HD 500 spectrometer fitted with a 5 mm PABBO BB/^{19}F-^{1}H/D-GRD probe, and equipped with a Bruker BCU-05 variable temperature unit. Measurements at temperature intervals of 5 K were collected in the temperature range from 300 to 340 K for the solution in C_6D_6 and from 300 to 320 K for the solution in $CDCl_3$. For C_7D_8, two distinct sets from 278 to 333 K and from 243 to 273 K were collected, the latter set using a cryostat Bruker

smart variable temperature unit (BSVT) and liquid nitrogen as cooling agent. For the toluene measurements, CH_3CN was used as an additional internal standard for line broadening analysis. ^1H NMR shifts were calibrated against known positions of solvent protons from incomplete deuteration. Fitting of NMR peaks was carried out using Bruker TopSpin 3.2 software and line broadening analysis was carried out using a combination of Lorentzian and Gaussian fit functions.[25,26]

2.2 Computational methods.

High level quantum chemical calculations have been performed using the GAMESS (US) program package,[27] version 1 May 2013, on various 32 and 64 bit Windows and Linux personal computers. The mixed basis sets LANL2DZ (Los Alamos National Laboratory 2 double ζ with optimized outer *p* functions, incorporating effective core potentials) for the transition metal Mo, and 6-31+G** (Pople double split valence set with added polarization and diffuse functions) for all other atoms have been employed.[28,29] The effect of dynamic electron correlation has been included with either density functional theory (DFT) or with 2nd order Møller-Plesset perturbation theory (MP2, frozen core). Consistent results and good performance were obtained with the hybrid-GGA (generalized gradient approximation) DFT functionals which include a percentage of Hartree-Fock exchange, B3LYP[30] and SOGGA11-X,[31] a modern functional that has the correct coefficient of the second order term. SOGGA11-X is apparently "the best in their class for simpler functional forms for chemical calculation of a broad variety of chemical problems".[31] We noted severe convergence problems calculating transition states of $MoO_2(acac)_2$ using various other density functionals, including advanced meta-GGA and hybrid-meta-GGA such as TPSS, M11 and M11-L. A possible explanation could include numerical instabilities related to the numerical integration of the kinetic energy density term contained in the meta functionals, possibly exacerbated by the diffuse basis functions, as noted in previous work.[32,33] Here, we consider the SOGGA11-X results as most reliable and provide B3LYP and MP2 values as an addition where appropriate.

Geometry optimizations were done with very tight convergence criteria (remaining gradients less than 10^{-6} Hartree $Bohr^{-1}$, OPTTOL=1E-6). The nature of stationary states (minimum structures or transition states) was confirmed by frequency calculations with numerical derivatives of the gradients, where positive and negative Cartesian displacements were enforced to increase the accuracy of the numerical Hessian calculation (NVIB=2). Vibrational scaling factors were used to partially compensate for anharmonicities and other effects for zero

point energies and thermodynamic properties, 0.959 for SOGGA11-X,[34] 0.964 for B3LYP and 0.941 for MP2.[35] Thermodynamic properties refer to 1 atm and 298.15 K using the usual ideal gas, rigid rotor and harmonic normal mode approximations in statistical thermodynamics. To evaluate solvent effects, some geometry searches and energy calculations were also performed using the SMD polarizable continuum solvation model.[36]

NMR chemical shifts were estimated with the gauge invariant atomic orbital (GIAO) method[37,38] at RHF level; in its present implementation, GAMESS does not permit the use of higher *ab initio* levels for GIAO calculations. Although at a low theory level, the calculated NMR shifts reported here satisfactorily reproduce the observed shifts (see below). Since in the liquid phase motional narrowing and averaging applies, we quote the isotropic shielding value of the chemical shielding tensor for comparison with experimental NMR spectra.

3. RESULTS AND DISCUSSION

3.1 Variable temperature NMR of $MoO_2(acac)_2$ in C_6D_6

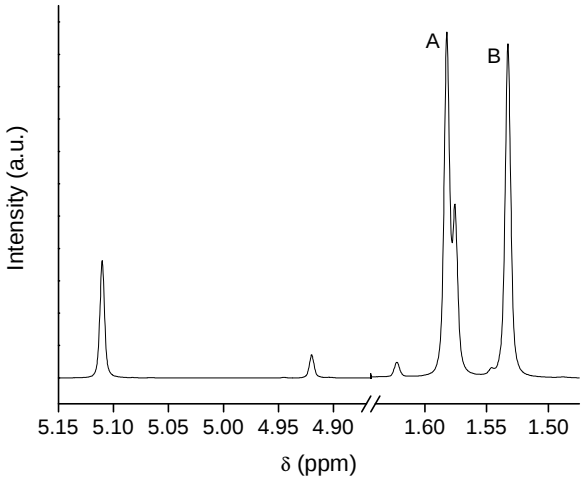

Figure 2. 500 MHz ^{1}H NMR spectrum of a $MoO_2(acac)_2$ solution in C_6D_6 (10^{-2} M) at 300 K (δ 5.11 (1H, s, CH), 1.58 (3H, s, CH_3), 1.53 (3H, s, CH_3); free Hacac (enol): 4.92 (1H, s, CH), 1.57 (2×3H, s, CH_3)).

Variable temperature NMR can be used to study the structure and dynamics of molecules and complexes, either by an analysis of relaxation rates[39,40] or by line shape analysis.[41,42] In this study, we use the latter approach. A representative ^{1}H NMR spectrum of a 10^{-2} M $MoO_2(acac)_2$ solution in C_6D_6 at 300 K is displayed in Fig. 2. The signal from the CH_3 groups of the acac ligand is given by two singlets at 1.58 and 1.53 ppm (here labeled as A and B respectively), whereas the signal from the CH unit is detected as a singlet at 5.11 ppm. It is possible to detect also the signal

of free, unbound, acetyl acetonate Hacac, with the enol tautomer at 1.57 ppm (2×CH_3 singlet) and 4.92 ppm (CH singlet). The detection of free Hacac from $MoO_2(acac)_2$ solutions in toluene has been previously reported[17,43] and we observed this effect to be even more marked for chloroform solutions.

In control tests, water or aqueous solutions of $HClO_4$ have been added to $MoO_2(acac)_2$ solutions in C_6D_6 or $CDCl_3$ which lead to the destruction of the Mo complexes, presumably by a hydrolysis reaction. However, we still detect free Hacac ligand even using dried solvent. Note that the presence of free Hacac does not affect our experiments negatively, but it can be used as internal standard for our line broadening analysis, as alternative to using CH_3CN.

3.1.1 Line broadening analysis

Variable temperature ^{1}H NMR spectra for a $MoO_2(acac)_2$ solution in C_6D_6 (10^{-2} M) for the region from 1.70 to 1.50 ppm are presented in Fig. 3. Increasing the temperature up to 340 K, a clear decrease of the frequency gap (here expressed in ppm, $\Delta\delta_{AB}$) between the two methyl groups of $MoO_2(acac)_2$ is detected, accompanied by an increase in the line broadening of the two signals. These combined effects are diagnostic of an equilibrium taking place with the two methyl groups exchanging between magnetically non-equivalent sites.[41]

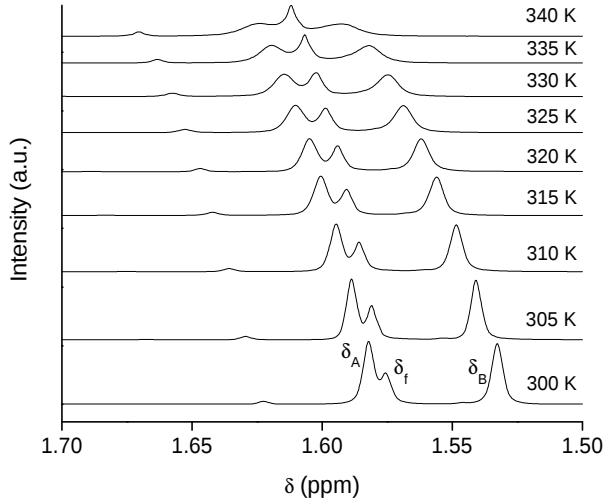

Figure 3. Variable temperature ^{1}H NMR for $MoO_2(acac)_2$ in C_6D_6. The two singlets at 300 K at 1.58 and 1.53 ppm are from the acac ligand. The singlet at 1.57 ppm is from the equivalent CH_3 groups of unbound, free acetyl acetonate Hacac (enol tautomer).

In order to determine the kinetic rate constant and activation energy of this exchange process, two approaches are commonly used in dynamic NMR: determination of the coalescence

temperature,[42] or line broadening analysis in a slow exchange regime, *i.e.* below the coalescence temperature.[44] The first approach is widely used[45] and assumes that both exchange sites are equally populated, *i.e.* $P_A = P_B$, where P_A and P_B are the populations of the sites A and B respectively (symmetric exchange).[46] At coalescence, the kinetic rate constant k of the symmetric exchange process at the coalescence temperature is directly proportional to the frequency difference of the two exchange sites A and B. The actual coalescence temperature depends on the strength of the applied magnetic field, the nature of the nuclei and the solvent used. In our case coalescence could not be reached at our operational NMR frequency (500 MHz), limited by a maximum heating temperature of *ca.* 10 K below the boiling point temperature of the solvent (for benzene T_b = 353 K). We therefore carried out a line broadening analysis instead, also to allow for the possibility of an asymmetric exchange. In a slow exchange regime (below coalescence) the broadening of the NMR signal is related to the rate constant of the exchange process between the two sites.[47] Without exchange, the width of the NMR signal at the half of its intensity, $W_{1/2}$, is reciprocal to the spin-spin relaxation time T_2. An exchange of nuclei between two different environments will shorten the residence lifetime τ_{ex} of the exchanging species in their respective environments which increases the line width $W_{1/2,\,ex}$. The rate constant k of the exchange process is equal to the reverse of the residence lifetime τ_{ex}.[48] Since usually $W_{1/2,ex} >> 1/T_2$, the approximation $1/T_2 = 0$ is often used.[49] In order to consider additional effects induced by field inhomogeneity, intrinsic (natural) line width and temperature, relative k values are commonly obtained subtracting from $W_{1/2,ex}$ the line width W_0 of a non-exchanging group used as reference, leading to Eq. 1,[50]

$$k = \pi\left(W_{1/2,ex} - W_0\right) \qquad \text{(Eq. 1)}$$

In the benzene and chloroform experiments, we use the equivalent methyl groups from free Hacac present in solution as reference for W_0. As the data analysis for the determination of kinetic parameters is based on line broadening, it is irrespective of signal intensity.[51] This is relevant since we observe an increase in the intensity of free Hacac by increasing the temperature (Fig. 3). Since previous experiments in excess of free Hacac did not detect any ligand exchange with the Mo center,[43] the only contribution to the line broadening of bound acac ligand in $MoO_2(acac)_2$ is the one induced by temperature towards the rate of exchange between two sites. To validate our approach, we have used both free Hacac and in addition CH_3CN as references in the toluene experiments (see below), without significant differences in the results.

3.1.2 Activation parameters for the exchange equilibrium of $MoO_2(acac)_2$ in C_6D_6

By using the data treatment described in the section above, line broadening, residence times and kinetic constants at different temperatures were determined (see Fig. S1 in the Supplementary Information for a representative line broadening fit using Gaussian and Lorentzian deconvolution). Temperature dependent kinetic rate constants *k* and further kinetic data for the exchange equilibrium of $MoO_2(acac)_2$ in benzene have been obtained by a line broadening analysis and are summarized in Table 1. An Arrhenius plot of ln *k* vs. 1/*T* (Fig. 4) provides the activation energy from the slope of the regression line, and a value of E_a = 70.8 ± 3.3 kJ mol^{-1} was obtained. These data are in agreement but improve the accuracy of previously reported values by Craven *et al.*[17] based on an analysis in benzene solution with CH_3CN as internal standard for the line broadening analysis. The similarities between our activation energy, obtained using the line broadening of free Hacac instead of CH_3CN, also proves that there is no exchange equilibrium between free and bound acac ligand, as such an equilibrium would have an additional broadening contribution and the two sets of data would not lead to similar activation parameters. This corroborates the studies by Zamaraev and co-workers[43] which did not detect an equilibrium between bound and free acac.

Table 1. Line broadening and kinetic data for CH_3 exchange in $MoO_2(acac)_2$ in benzene, using free Hacac ligand as internal standard.

T (K)	$W_{\frac{1}{2},ex,A}$ (Hz) [a]	$W_{\frac{1}{2},ex,B}$ (Hz) [b]	$W_{\frac{1}{2},0}$ (Hz) [c]	$\overline{W}_{\frac{1}{2},ex,cor}$ (Hz) [d]	τ_{ex} (s) [e]	k (s^{-1}) [f]
300	2.39	2.45	2.28	0.14	2.29	0.44
305	2.28	2.40	2.08	0.26	1.21	0.83
310	2.60	2.77	2.26	0.43	0.75	1.34
315	3.06	3.18	2.39	0.73	0.44	2.28
320	3.23	3.60	2.54	0.87	0.37	2.73
325	3.85	4.26	2.81	1.24	0.26	3.89
330	4.63	4.91	3.12	1.65	0.19	5.19
335	5.46	5.65	2.69	2.87	0.11	9.01
340	7.77	8.07	2.53	5.39	0.06	16.94

[a] broadening of peak A from Fig. 3;
[b] broadening peak B from Fig. 3;
[c] broadening of the methyl groups of the free Hacac;
[d] average of the broadening of peaks A and B, with broadening of the free Hacac subtracted;
[e] residence time;
[f] kinetic constant given as reciprocal of residence time.

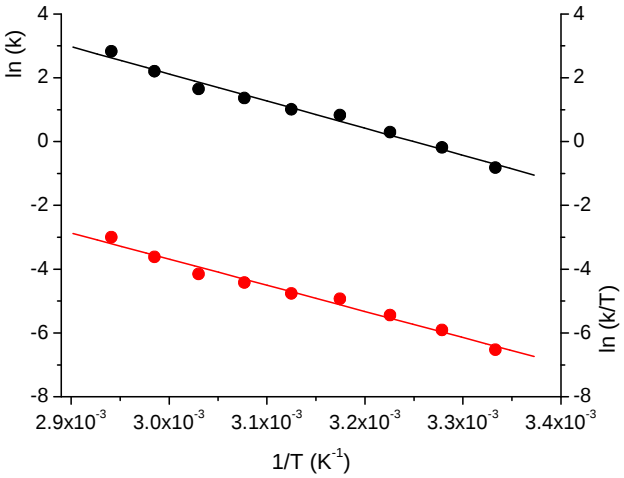

Figure 4. Y-axis on the left: (●) Arrhenius plot for the equilibrium process involving the CH_3 groups of $MoO_2(acac)_2$ in benzene, from 300 to 340 K. Linear regression parameters are (temperature T in K): $\ln k = -8.52 \cdot 10^3\ 1/T + 27.7$ ($R^2 = 0.984$).
Y-axis on the right: (●) Eyring–Polanyi plot for the same equilibrium; linear regression yields $\ln (k/T) = -8.20 \cdot 10^3\ 1/T + 20.9$ ($R^2 = 0.983$).

Since the exchange mechanism is based on unimolecular reactions, further analysis was carried out using transition state theory based on the Eyring–Polanyi equation (Eq. 2),

$$\ln \frac{k}{T} = -\frac{\Delta H^{\ddagger}}{R} \cdot \frac{1}{T} + \ln \frac{k_B}{h} + \frac{\Delta S^{\ddagger}}{R} \qquad \text{(Eq. 2)}$$

where the symbols have their usual meaning.[52] An Eyring–Polanyi plot of $\ln(k/T)$ vs. $1/T$ (Fig. 4) yields the activation enthalpy $\Delta H^{\ddagger}$ and entropy $\Delta S^{\ddagger}$ for the exchange process, $\Delta H^{\ddagger} = 68.1 \pm 3.4$ kJ mol^{-1}, and $\Delta S^{\ddagger} = -24 \pm 8.3$ J mol^{-1} K^{-1}. These data are again in agreement but improve the accuracy of previously reported values by Craven *et al.*[17] (note that $\Delta S^{\ddagger}$ was reported as positive where the plus sign is clearly a typo, as can be seen by re-analysing the original raw data)

3.2 Variable temperature NMR of $MoO_2(acac)_2$ in $CDCl_3$

To assess possible solvent effects, a set of dynamic NMR data was collected using deuterated chloroform as a solvent for $MoO_2(acac)_2$ (10^{-2} M), see Fig. 5. Compared with benzene as solvent, coalescence is nearly reached at 320 K, and changes in chemical shift by temperature are small. In addition, a larger chemical shift for the methyl signals towards higher field values is noted. This is consistent with previous studies of solvent effects on CH_3 groups adjacent to carbonyl groups, and may be due to a lone-pair/aromatic ring interaction between the benzene aromatic ring and the carbonyl group.[53]

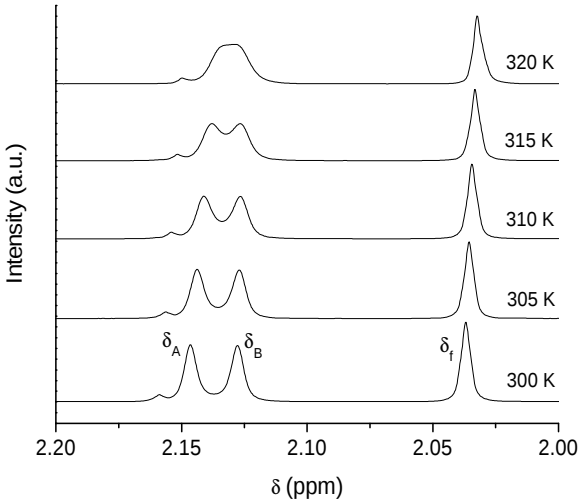

Figure 5. Variable temperature ^{1}H NMR for $MoO_2(acac)_2$ in $CDCl_3$. The two singlets at 2.14 and 2.13 ppm are from the acac ligand, the singlet at 2.04 ppm from the equivalent CH_3 groups of unbound Hacac.

Applying a line broadening analysis using the free Hacac as reference, temperature dependent kinetic data have been obtained as summarized in Table 2 (see Fig. S2 in the Supplementary Information for a representative line broadening fit). Using these temperature dependent k values, the Arrhenius activation energy E_a and the thermodynamic activation parameters $\Delta H^{\ddagger}$ and $\Delta S^{\ddagger}$ for the exchange equilibrium process are obtained by an Arrhenius and Eyring–Polanyi plot (see Fig. 6), yielding E_a = 57.5 ± 3.4 kJ mol^{-1}, $\Delta H^{\ddagger}$ = 54.9 ± 3.4 kJ mol^{-1} and $\Delta S^{\ddagger}$ = -54.7 J ± 10 J mol^{-1} K^{-1}.

Table 2. Line broadening and kinetic data for CH_3 exchange of $MoO_2(acac)_2$ in chloroform, using free Hacac ligand as internal standard. The experimental point at 320 K was not inserted as the merging of the peaks did not give sufficient deconvolution parameters.

T (K)	$W_{\frac{1}{2},ex,A}$ (Hz) [a]	$W_{\frac{1}{2},ex,B}$ (Hz) [b]	$W_{\frac{1}{2},0}$ (Hz) [c]	$\overline{W}_{\frac{1}{2},ex,cor}$ (Hz) [d]	τ_{ex} (s) [e]	k (s^{-1}) [f]
300	2.79	2.81	2.08	0.72	0.44	2.26
305	3.25	3.25	2.13	1.12	0.28	3.52
310	3.79	3.76	2.13	1.65	0.19	5.18
315	4.34	4.35	2.21	2.14	0.15	6.71

[a] broadening of peak A from fig. 5;
[b] broadening peak B from fig. 5;
[c] broadening of the methyl groups of the free Hacac;
[d] average of the broadening of peaks A and B, with broadening of the free Hacac subtracted;
[e] residence time;
[f] kinetic constant given as reciprocal of residence time.

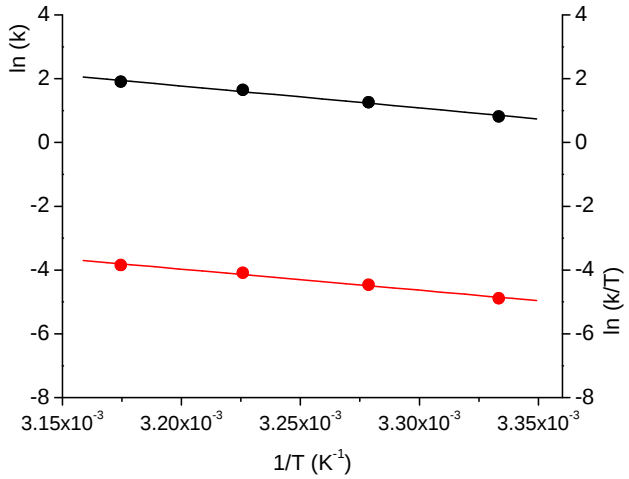

Figure 6. Y-axis on the left: (●) Arrhenius plot for the equilibrium process involving the CH_3 groups of $MoO_2(acac)_2$ in chloroform, from 300 to 315 K. Linear regression parameters are (temperature T in K): $\ln k = -6.92 \cdot 10^3\ 1/T + 23.9$ ($R^2 = 0.990$).
Y-axis on the right: (●) Eyring–Polanyi plot for the same equilibrium; linear regression yields $\ln (k/T) = -6.60 \cdot 10^3\ 1/T + 17.2$ ($R^2 = 0.988$).

3.3 Variable temperature NMR of $MoO_2(acac)_2$ in C_7D_8

A final set of measurements was carried out using dried, deuterated toluene as solvent and the addition of CH_3CN as internal standard for line broadening. In our analysis, we use both unbound Hacac and CH_3CN as internal standards to compare the different approaches and also to validate our use of Hacac in the previous experiments. With toluene, we have also expanded the temperature range of the variable temperature NMR in an attempt to further improve the accuracy of activation parameters in the line broadening analysis. Experimental data were divided in two sets, a set from 278 to 333 K and a set from 243 to 273 K at 5 K intervals. Representative NMR spectra are displayed in Fig. 7 showing the acac ligands and Hacac. Expanded spectra also showing the CH_3CN peak are displayed in the Supplementary Information (Fig. S3). In this experiment, we have used freshly sublimed $MoO_2(acac)_2$ and carefully dried solvent to assess whether it is possible to significantly reduce the amount of free Hacac. However, we still detect the presence of free Hacac (see Fig. 7), despite our precautions. Note that free Hacac was also previously detected by Craven *et al.*[17]

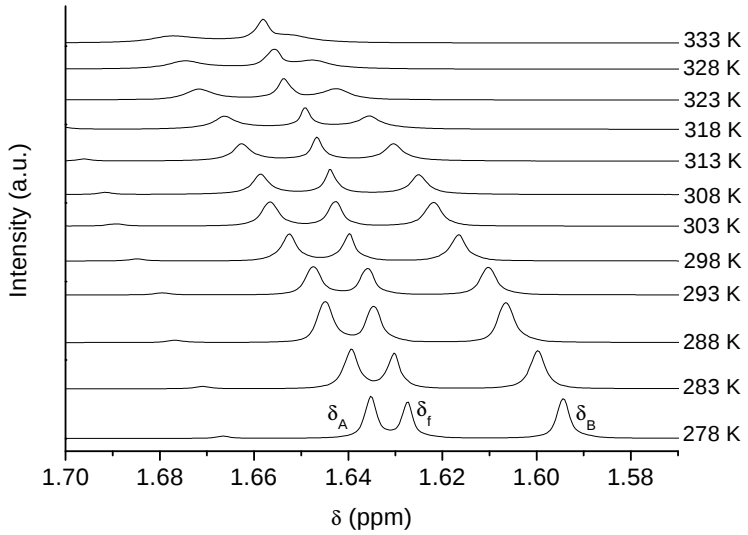

Figure 7. Variable temperature ^{1}H NMR for $MoO_2(acac)_2$ in C_7D_8. The two singlets at 1.63 and 1.59 ppm are from the acac ligand, the singlet at 1.63 ppm from the equivalent CH_3 groups of unbound Hacac.

We applied a line broadening analysis using both free Hacac and CH_3CN as reference without significant differences between both approaches. Temperature dependent kinetic data have been obtained as summarized in Table 3 (see Fig. S4 in the Supplementary Information for representative line broadening fits). Below about 293 K, the contribution of exchange to line broadening becomes very small and difficult to determine by the line shape. Extension of the temperature range below 293 K therefore does not improve the determination of kinetic and activation parameters, and we have limited the line shape analysis to the 293 to 328 K range. The final data point at 333 K was not included due to the overlap of the signal of free Hacac and bound acac. The activation energy for the $MoO_2(acac)_2$ equilibrium using the Arrhenius plot (Fig. 8 a) is $E_{a,Hacac}$ = 60.7 ± 2.9 kJ mol^{-1} and E_{a,CH_3CN} 65.4 ± 2.5 kJ mol^{-1} using Hacac and CH_3CN respectively as reference standards, giving a mean value of E_a = 63.1 kJ mol^{-1}. The values overlap within their uncertainty limits, thus validating our approach of using Hacac with benzene and chloroform as solvents. Comparing with benzene and chloroform, the following trend is observed: $E_{a,C6D6}$ = 70.8 kJ mol^{-1}, $E_{a,C7D8}$ = 63.1 kJ mol^{-1} and $E_{a,CDCl3}$ = 57.5 kJ mol^{-1}, which suggests a dependency of the activation energy on the polarity of the medium. By using the Eyring-Polanyi plot (Fig. 8 b) activation enthalpies are $\Delta H^{\ddagger}_{Hacac}$ = 58.2 ± 2.9 kJ mol^{-1} and $\Delta H^{\ddagger}_{CH_3CN}$ = 62.9 ± 2.9 kJ mol^{-1}, and activation entropies are $\Delta S^{\ddagger}_{Hacac}$ = -50.1 ± 9.3 J mol^{-1} K^{-1} and $\Delta S^{\ddagger}_{CH_3CN}$ = -35.0 ± 7.5 J mol^{-1} K^{-1} using Hacac and CH_3CN respectively as reference standard, giving mean values of $\Delta H^{\ddagger}_{Hacac}$ = 60.6 kJ mol^{-1} and $\Delta S^{\ddagger}_{Hacac}$ = -42.6 J mol^{-1} K^{-1}.

Table 3. Line broadening and kinetic data for CH_3 exchange in $MoO_2(acac)_2$ in toluene, using free Hacac ligand and CH_3CN internal standard.

T (K)	$W_{\frac{1}{2},ex,A}$ (Hz) [a]	$W_{\frac{1}{2},ex,B}$ (Hz) [b]	$W_{\frac{1}{2},0,\mathrm{Hacac}}$ (Hz) [c]	$W_{\frac{1}{2},0,\mathrm{CH3CN}}$ (Hz) [c]	$\overline{W}_{\frac{1}{2},ex,cor,\mathrm{HACAC}}$ (Hz) [d]	$\overline{W}_{\frac{1}{2},ex,cor,\mathrm{CH3CN}}$ (Hz) [d]	$\tau_{ex,\mathrm{Hacac}}$ (s) [e]	$\tau_{ex,\mathrm{CH3CN}}$ (s) [e]	$k_{,\mathrm{Hacac}}$ (s^{-1}) [f]	$k_{,\mathrm{CH3CN}}$ (s^{-1}) [f]
278	1.398	1.481	1.256	1.272	0.1835	0.1675	1.73	1.90	0.58	0.53
283	1.732	1.796	1.569	1.576	0.195	0.188	1.63	1.69	0.61	0.59
288	2.019	2.189	1.934	1.917	0.17	0.187	1.87	1.70	0.53	0.59
293	1.765	1.848	1.604	1.640	0.202	0.166	1.57	1.91	0.64	0.52
298	1.838	1.903	1.527	1.554	0.343	0.316	0.93	1.01	1.08	0.99
303	1.945	1.987	1.603	1.601	0.363	0.365	0.88	0.87	1.14	1.15
308	2.198	2.25	1.605	1.533	0.619	0.691	0.51	0.46	1.94	2.17
313	2.536	2.652	1.612	1.563	0.982	1.031	0.32	0.31	3.09	3.24
318	3.086	3.354	1.649	1.646	1.571	1.574	0.20	0.20	4.94	4.94
323	3.755	3.695	1.757	1.685	1.968	2.04	0.16	0.16	6.18	6.41
328	5.063	4.417	1.95	1.733	2.79	3.007	0.11	0.11	8.77	9.45

[a] broadening of peak A from fig. 7;
[b] broadening peak B from fig. 7;
[c] broadening of the methyl groups of the free Hacac or CH_3CN standard;
[d] average of the broadening of peaks A and B, with broadening of the free Hacac or CH_3CN subtracted;
[e] residence time;
[f] kinetic constant given as reciprocal of residence time.

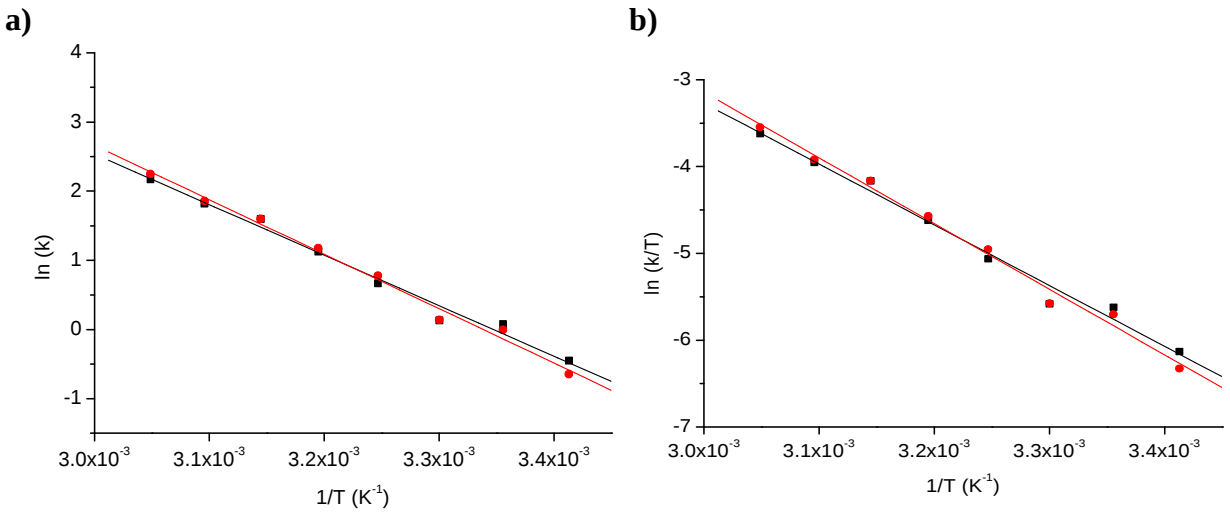

Figure 8. a) Arrhenius plot for the equilibrium process involving the CH_3 groups of $MoO_2(acac)_2$ in toluene, from 293 to 328 K using (■) free Hacac as reference and (●) CH_3CN as standard. Linear regression parameters are (temperature T in K): $\ln k = -7.31 \cdot 10^3\ 1/T + 24.5$ ($R^2 = 0.987$), and $\ln k = -7.87 \cdot 10^3\ 1/T + 26.3$ ($R^2 = 0.991$) for free Hacac and CH_3CN as standard, respectively. b) Eyring–Polanyi plot using (■) free Hacac as standard and (●) CH_3CN as standard. Linear regression parameters are (temperature T in K): $\ln (k/T) = -6.99 \cdot 10^3\ 1/T + 17.7$ ($R^2 = 0.985$). and $\ln (k/T) = -7.56 \cdot 10^3\ 1/T + 19.5$ ($R^2 = 0.991$) for free Hacac and CH_3CN as standard, respectively.

Based on the experimental evidence, the following conclusions can be drawn: it appears likely that the ground state of $MoO_2(acac)_2$ in solution has a *cis*-conformation with two equivalent enantiomers. The two acac methyl groups in the *cis*-conformation are in different chemical environments and have thus two NMR peaks. Due to a symmetric exchange mechanism, these peaks coalesce at elevated temperatures. In principle four exchange processes appear conceivable: (i) methyl group migration, (ii) oxo dissociation to give a five coordinate intermediate, (iii) complete dissociation of the ligand and (iv) a twist mechanism with exchange of methyl groups without metal-ligand bond breaking. Case (i) can be ruled out by energy considerations, and so far any reaction involving the acac ligand bound to a transition metal always involved the hydrogen of the CH group and not of the methyl groups.[19] The slightly negative activation entropy indicates that the transition state linking the two enantiomers is more rigid or sterically constrained than the ground state;[54] the transition state is presumably not a dissociative state since this usually gives large positive activation entropies. The similarity of activation parameters in different solvents which have distinctively different dipole moments suggests also that the transition state does not include charged species,[55] although a trend can be seen with the more polar environment decreasing the activation energy E_a. These considerations seem to rule out cases (ii) and (iii), and leave case (iv) as the most likely mechanism.

3.4 Quantum chemical calculations on $MoO_2(acac)_2$

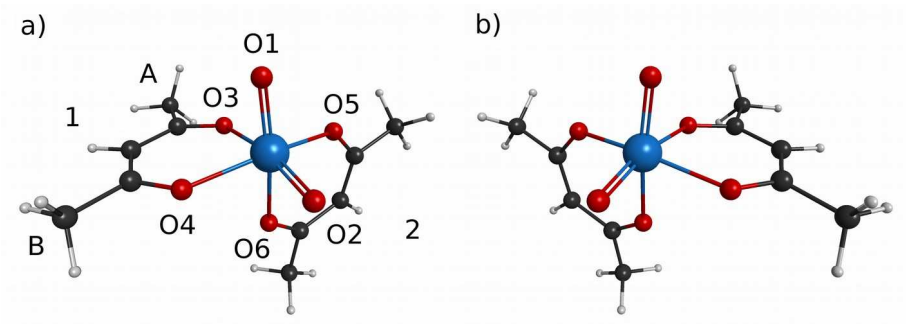

Figure 9. *Ab initio* structures of the ground state enantiomers of the $MoO_2(acac)_2$ complex (C_2 symmetry), a) Λ-*cis*-$MoO_2(acac)_2$ and b) Δ-*cis*-$MoO_2(acac)_2$.

If not noted otherwise, all results refer to the SOGGA11-X/LANL2DZ,6-31+G** level without solvent model. The *ab initio* structure of the ground state minimum (all frequencies real) of the $MoO_2(acac)_2$ complex is shown in Fig. 9. The structure has a *cis* configuration of the two O ligands (O1, O2) with a chiral C_2 symmetry. The oxygens bind to the central Mo in a slightly distorted octahedral symmetry, with a bond angle between the O ligands and Mo of 105.1° and an

Mo-O bond distance of 1.69 Å (104.9°/1.71 Å for B3LYP, 102.4°/1.78 Å for MP2, respectively). The oxygens of the two acac ligands are a bit further away from the Mo reflecting the reduced bond order, with r_{Mo-O3} = 2.25 Å and r_{Mo-O4} = 2.03 Å (2.25/2.04 Å for B3LYP, 2.29/2.05 Å for MP2, respectively). The O of one acac form a bond angle of 80.4° with the Mo (79.9° B3LYP, 81.1° MP2). The two ends of one acac unit, *e.g.*, A and B, are not equivalent since they are in a slightly different chemical environment, with A being near just one O ligand (O1), whereas B is near both O ligands (and correspondingly for the other acac). The planes of the acac units are almost perpendicular to each other. If θ is defined as the dihedral angle of the acac oxygens O6-O5-O4-O3 (approximately the torsional angle between the two acac), then θ = -89.2° is found for Λ-*cis*-$MoO_2(acac)_2$ (-88.6° B3LYP, -89.3° MP2).

Due to almost free rotation, the ^{1}H NMR signals of a methyl group will average to one single peak, with a peak separation between methyl group A (and the corresponding methyl group of acac 2) and the non-equivalent group B (and the corresponding methyl group of acac 2). The GIAO calculations at RHF level provide NMR chemical shielding values. To convert this into NMR chemical shifts in the conventional ppm scale, we also calculated NMR shielding values for free Hacac (enol tautomer), and calibrated all calculated ^{1}H NMR shifts against the observed value for the CH group of Hacac in benzene, 4.92 ppm. Against this calibration standard, the calculated ^{1}H NMR shift of the equivalent CH groups of the two acac groups is 5.31 ppm, compared with 5.78 ppm measured. The averaged shifts of the A methyl groups is 1.89 ppm (2.14 ppm measured for δ_A), and for the B is 1.87 ppm (2.13 ppm measured for δ_B). Taking into account the low level of theory, the neglect of solvent in the calculation and the known shortcomings of *ab initio* NMR calculations in general, satisfactory agreement between theory and experiment is found, explaining the small splitting of methyl group signals found in the experiment and corroborating the quantum chemical calculation of a ground state chiral C_2 symmetry *cis*-$MoO_2(acac)_2$ complex.

The two chiral enantiomers interconvert *via* transition states. It is very relevant to locate these states to understand the dynamics and the stability of the chiral complex. In a systematic search of the potential energy landscape between Mo and its ligands, we used starting geometries with several unrestricted *cis* and *trans* configurations in saddle point searches, and various symmetry restricted configurations based on chemical intuition (*e.g.*, C_{2v} for *cis*, and C_i and D_{2h} for *trans*) for optimizations. For all stationary geometries found, subsequent frequency calculations were performed to confirm the presence of a transition state (one imaginary

frequency) and to obtain thermodynamic data. In addition, either relaxed potential energy scans or intrinsic reaction coordinate (IRC) calculations[56,57] were performed to confirm that the transition states indeed connect the two ground state enantiomers. The lowest transition state located, TS1, is shown in Fig. 10 (one imaginary frequency).

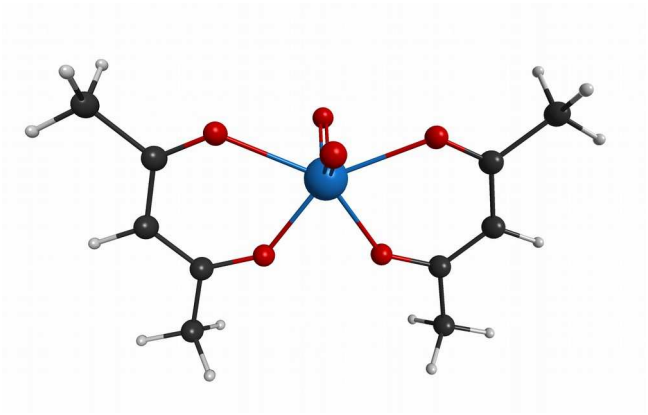

Figure 10. *Ab initio* structure of the lowest *cis* transition state of $MoO_2(acac)_2$, TS1.

In this configuration, the O ligands are *cis* as in the ground state. The configuration is almost C_{2v}, with θ = 1.3° (0.9° for B3LYP, 1.7° for MP2). C_{2v} would have θ = 0°. We have also located a stationary state with almost the same geometry at θ = 0°, with slightly lower energy (-0.2 kJ mol^{-1}) and all frequencies real. It is not clear to us whether this local minimum is just an artifact of the symmetry restricted calculation or genuine. We have performed a relaxed potential energy scan as a function of θ (see Fig. 11) which confirms that both ground state enantiomers are connected *via* TS1. Since TS1 and the local minimum (if genuine) are so close in geometry and energy, TS1 will be effectively the lowest energy transition state linking the enantiomers. Compared to the ground state, TS1 has ΔE_{el} = 81.5 kJ mol^{-1}, ΔE_0 = 81.3 kJ mol^{-1} (where ΔE_0 includes electronic energy and zero-point energy), $\Delta H°$ = 79.1 kJ mol^{-1} and $\Delta S°$ = -11.7 J mol^{-1} K^{-1} (B3LYP values are 80.1, 77.5 and 76.7 kJ mol^{-1}, and +6.4 J mol^{-1} K^{-1}, MP2 values are 98.0, 100.3 and 99.4 kJ mol^{-1}, and +13.3 J mol^{-1} K^{-1}).

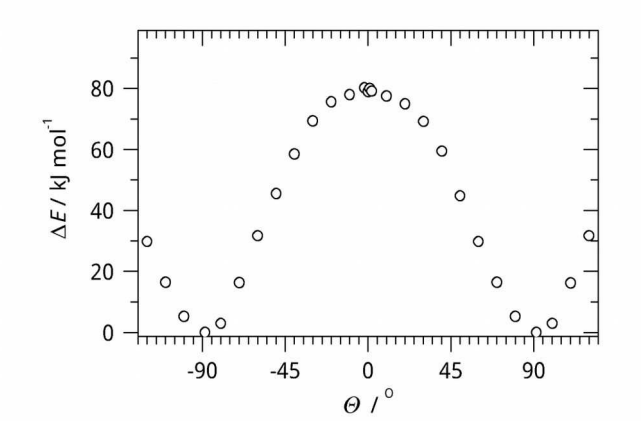

Figure 11. Relaxed potential energy scan as a function of θ (approximately the torsional angle between the acac units) showing the interconversion of the two enantiomers of ground state $MoO_2(acac)_2$ *via* the transition state TS1.

Slightly higher in energy, two further transition states (one imaginary frequency) have been found, TS2a and TS2b, see Fig. 12. They are close in energy, with the main difference being the position of the O ligands with respect to the acac units. TS2a has ΔE_{el} = 109.9 kJ mol^{-1}, ΔE_0 = 111.9 kJ mol^{-1}, $\Delta H°$ = 107.8 kJ mol^{-1} and $\Delta S°$ = 109.9 J mol^{-1} K^{-1}, and TS2b ΔE_{el} = 114.7 kJ mol^{-1}, ΔE_0 = 114.0 kJ mol^{-1}, $\Delta H°$ = 111.9 kJ mol^{-1} and $\Delta S°$ = -50.3 J mol^{-1} K^{-1}. For completeness, the corresponding values for B3LYP are 106.3, 106.4, 103.7 kJ mol^{-1} and -24.7 J mol^{-1} K^{-1} for TS2a, and 110.2, 106.1, 105.8 kJ mol^{-1} and +6.4 J mol^{-1} K^{-1} for TS2b; for MP2 they are 111.1, 112.3, 109.0 kJ mol^{-1} and -37.3 J mol^{-1} K^{-1} for TS2a, and 115.9, 111.4, 111.4 kJ mol^{-1} and +16.1 J mol^{-1} K^{-1} for TS2b.

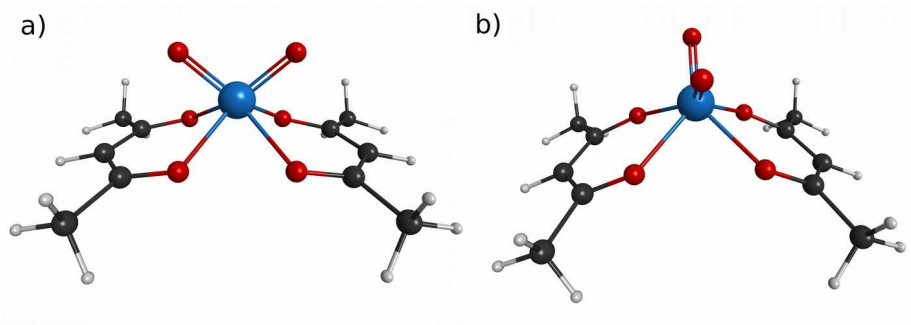

Figure 12. *Ab initio* structures of a set of higher *cis* transition states of $MoO_2(acac)_2$, TS2a and TS2b (C_{2v} symmetry).

$MoO_2(acac)_2$ is quite often depicted as a *trans* complex of D_{2h} symmetry, as in Fig. 1c. The quantum chemical calculations clearly show, however, that all lower energy configurations are *cis*, and that the *trans* position of the oxygen ligands involves a heavy energy penalty. Our search for *trans* stationary states proved to be difficult, since without symmetry constraints, all optimizations went back to the *cis* ground state. Only B3LYP was able to locate a *trans* transition

state of C_i symmetry (one imaginary frequency) which is ΔE_{el} = 214.7 kJ mol^{-1} above the ground state (TS3, see Fig. 13). TS3 is a transition state linking the two ground state enantiomers, as shown by an IRC calculation. A symmetry constrained search also obtained the D_{2h} *trans* stationary state ΔE_{el} = 230.7 kJ mol^{-1} above the ground state; with 5 imaginary frequencies, however, this is only a higher-order saddle point, not a transition state.

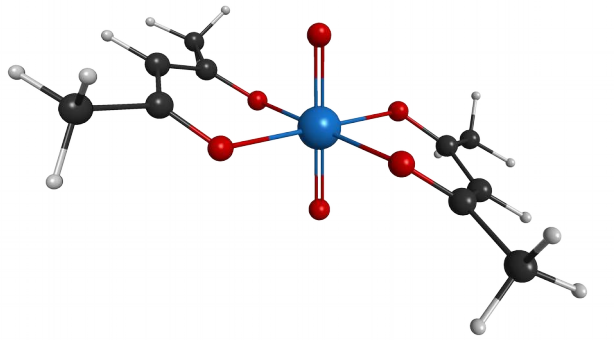

Figure 13. *Ab initio* structure (B3LYP) of the lowest *trans* stationary configuration of $MoO_2(acac)_2$, TS3 (C_i symmetry).

3.5 Racemization mechanisms in $MoO_2(acac)_2$

According to the calculations, the interconversion of enantiomers occurs by a twisting mechanism and alignment of the two acac ligands without breaking bonds, to form a symmetric, achiral transition state, while the oxygen ligands stay in the *cis* configuration (except for the high energy TS3). Since the two oxygen ligands stay *cis*, as if they would be held in place by being part of a bidentate, the situation resembles chiral tris-chelate, octahedral ligands ML_3, which are known to racemize *via* the Ray-Dutt or the Bailar twist mechanisms.[58-60]Similar twist mechanisms may thus be expected to apply to $MoO_2(acac)_2$ as well. Looking at the planes of each bidentate ligand, in the Bailar mechanism of racemization, each plane turns synchronously in one direction (say clockwise) through an achiral, trigonal prismatic transition state of D_3 symmetry. For $MoO_2(acac)_2$, an equivalent mechanism applies *via* TS2b (see Fig. 12b); since the two oxygens ligands are different to the bidentate acac units, TS2b has C_{2v} symmetry instead of D_3 which ML_3 would have. In the Ray-Dutt mechanism of racemization, two bidentate ligand planes turn in the same direction (say clockwise), while the third ligand turns in the opposite direction (say counter-clockwise) through an achiral transition state of C_{2v} symmetry. An equivalent mechanism applies to $MoO_2(acac)_2$ *via* TS2a (see Fig. 12a), where the two oxygen ligands play the role of the counter-moving bidentate.

The lowest energy racemization route for $MoO_2(acac)_2$ occurs *via* TS1 and with a twist mechanism which to our knowledge has not been described before. In this mechanism, the two oxygens of the two acac units (O4 and O5 in Fig. 9) which are in-between the two O ligands (O1, O2) remain locked in this position, while the two opposing oxygens of the acac units (O3, O6) move towards each other until the two acac units are in one plane in a C_{2v} transition state (see Fig. 10). Such a mechanism is unlikely to be relevant for an octahedral ML_3 complex, where all ligands (and thus all oxygens) are equivalent, but in $MoO_2(acac)_2$, the O are bonded differently to Mo than the acac oxygens and so they are not equivalent.

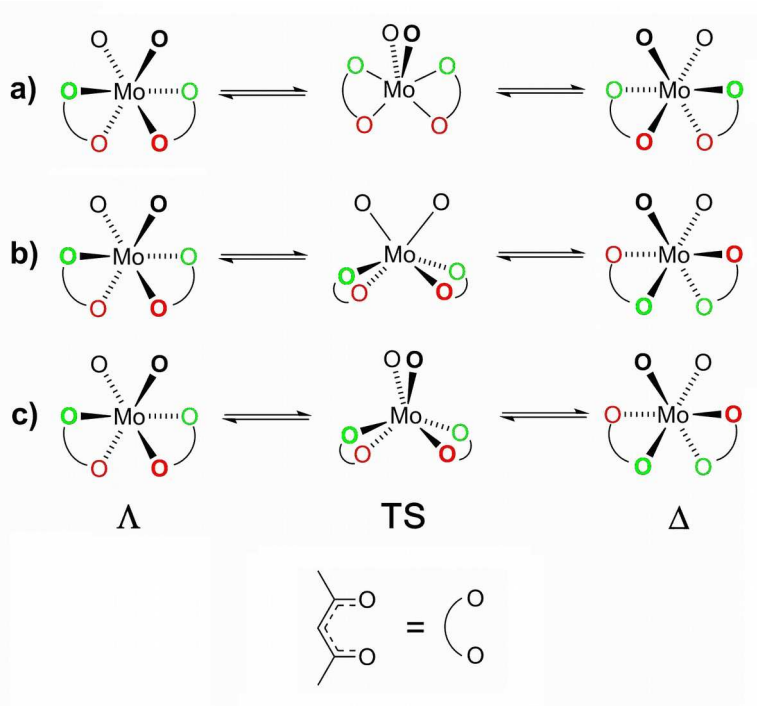

Figure 14. Schematic showing relevant racemization pathways *via* twisting mechanisms, viewed along a C_3 rotation axis of the pseudo-octahedral ground state. Red label: acac end initially in position A in Λ (being near just one O ligand, as in fig. 9); green label: acac end initially in position B in Λ (near both O ligands). **a)** Mechanism proposed in the present work (TS1), **b)** Ray-Dutt type (TS2a), and **c)** Bailar type mechanism (TS2b).

For convenience, a summary for all three racemization mechanisms is shown schematically in Fig. 14. It is important to note that in the newly described mechanism, the methyl groups stay in their position A or B after conversion (see Fig. 14 a), which would lead to additional broadening of NMR peaks at elevated temperatures, but not to a coalescence of peaks A and B. This is contrary to the NMR experiment. In the Ray-Dutt and Baylar mechanisms, however, the methyl groups change their environment from A to B and vice versa (see Fig. 14 b

and c) which would lead to the observed coalescence. Although TS1 is calculated to be the lowest transition state linking the two enantiomers, the mechanism *via* TS1 does not seem to be compatible with the observed coalescence of NMR peaks. The calculations refer to the isolated gas phase, whereas the experiment was performed in solution. Our current conclusion is that the energies of the three transition states are relatively close (ΔE_0 = 81-114 kJ mol^{-1} for SOGGA-11X, 100-112 kJ mol^{-1} for MP2), and that the true order and relevance of transition states may be reversed in the solution due to solution effects. In any case, the observed negative entropy change reflects the fact that transition states TS1 and also TS2a and TS2b are slightly tighter than the ground state, with slightly higher intermolecular frequencies.

We also tried to reproduce the solvent effects that lead to the observed variation of activation parameters and possibly the changed order of transition states using a polarizable continuum solvent model (SMD). The energy of solvation is significant for the Mo complex, but it turns out that in taking the difference between the ground state and the various transition states, solvent effects almost completely cancel out. The calculated ΔE_{el} of TS1, *e.g.*, is 81.8 kJ mol^{-1} in benzene and 79.8 kJ mol^{-1} in chloroform, almost unchanged from the isolated value of 81.5 kJ mol^{-1}. It is thus clear that the observed solvent effects are mainly due to individual solvent molecule interactions with the Mo complex beyond the polarizable continuum model.

4. SUMMARY AND CONCLUSIONS

The stereochemistry and dynamics of $MoO_2(acac)_2$ in benzene, chloroform and toluene was investigated by variable temperature ^{1}H NMR, density functional theory and *ab initio* methods. In solution, an equilibrium between two chiral enantiomers with C_2 symmetry was identified, Λ-*cis*-$MoO_2(acac)_2$ and Δ-*cis*-$MoO_2(acac)_2$. The two enantiomers are connected *via* an achiral *cis* transition states with effectively C_{2v} symmetry that could switch the two enantiomeric conformations *via* a twist mechanism of the acac ligands. The calculations identify three possible mechanisms *via* different transition states, according to the Ray-Dutt and Bailar mechanisms, and a newly described mechanism. Among these mechanisms, only Ray-Dutt and the Bailar mechanism are compatible with the observed coalescence of NMR peaks. Activation parameters E_a, $\Delta H^‡$, and $\Delta S^‡$ were experimentally determined for this exchange process, with a small, negative $\Delta S^‡$, and a positive $\Delta H^‡$ of 68.1 kJ mol^{-1} in benzene, 54.9 kJ mol^{-1} in chloroform, and 60.6 kJ mol^{-1} in toluene, in reasonable general agreement with the calculations. *trans*

configurations of $MoO_2(acac)_2$ are very much higher in energy than *cis*. According to the calculations and the experimental analysis, the enantiomers interconvert within seconds near room temperature, and much faster at elevated temperatures. Racemization will thus prevent the use of enantiomerically pure $MoO_2(acac)_2$ for chiral catalysis under practical conditions, which explains why chiral $MoO_2(acac)_2$ in solution is not capable to lead to any evident enantiomeric excess for epoxidation unless chiral ligands are used. The insights gained in the present work on the stereochemistry and dynamics of chiral $MoO_2(acac)_2$ will be useful for future Mo catalyst design which might provide attractive alternative routes for chiral epoxidation reactions, for example by functionalizing the acac ligands.

ACKNOWLEDGEMENTS

We are grateful to Dr. Michael Morris, Dr. Grant Hill and Prof. Iain Coldham (University of Sheffield) for helpful discussions. This work is supported financially by the University of Sheffield, including a start-up grant to MC (CHM-313072).

SUPPORTING INFORMATION

Representative Gaussian and Lorentzian fitting deconvolutions for line broadening analysis, NMR spectra including acetonitrile peak using toluene as a solvent, low temperature ^{1}H NMR data between 273 and 243 K and ln(k) against 1/T for $MoO_2(acac)_2$ in toluene; optimized SOGGA11X geometries with 6-31G+** and modified LANL2DZ on Mo; typical input file for GAMESS calculations; original data set from Craven *et al.* (ref. 17) for $MoO_2(acac)_2$ exchange in benzene solution.

REFERENCES

1 Gouzerh, P.; A. Proust, A. Main-Group Element, Organic, and Organometallic Derivatives of Polyoxometalates. *Chem. Rev.* **1998**, 98, 77–111.

2 Korstanje, T. J.; Folkertsma, E.; Lutz, M.; Jastrzebski, J. T. B. H.; R. J. M. Klein Gebbink, R. J. M. Synthesis, Characterization, and Catalytic Behavior of Dioxomolybdenum Complexes Bearing Acac-Type Ligands. *Eur. J. Inorg. Chem.* **2013**, 2195–2204.

3 Zhang, C.; Rheinwald, G.; Lozan, V.; Wu, B.; Lassahn, P.-G.; Lang H.; Janiak, C. Structural Study and Solution Integrity of Dioxomolybdenum (VI) Complexes with Tridentate Schiff Base and Azole Ligands. *Z. Anorg. Allg. Chem.* **2002**, 628, 1259–1268.

4 S. N. Rao, S. N.; Munshi, K. N.; Rao, N. N.; Bhadbhade M. M.; Suresh, E. Synthesis, Spectral and X-ray Structural Characterization of [*cis*-MoO_2(L)(solv)](L=salicylidene salicyloyl hydrazine) and its Use as Catalytic Oxidant. *Polyhedron*, **1999**, 18, 2491–2497.

5 Calvente, R. M.; Campos-Martin J. M.; Fierro, J. L. G. Effective Homogeneous Molybdenum Catalyst for Linear Terminal Alkenes Epoxidation with Organic Hydroperoxide. *Catal. Commun.* **2002**, 3, 247–251.

6 Arnold, U.; Habicht W.; Döring, M. Metal-Doped Epoxy Resins: New Catalysts for the Epoxidation of Alkenes with High Long-Term Activities. *Adv. Synth. Catal.* **2006**, 348, 142–150.

7 Tani, K.; Hanafusa M.; Otsuka, S. Asymmetric Epoxidation of Hydrocarbon Olefins by Full-size *tert*-butyl hydroperoxide with Molybdenum(VI) Catalysts in the Presence of Optically Active Diols. Application to the Asymmetric Synthesis of (3S)-2,3-oxidosqualene. *Tetrahedron Lett.* **1979**, 20, 3017–3020.

8 Kotov, S. V. ; Kolev T. M.; Georgieva, M. G. Preparation and Use of Novel Molybdenum-Containing Organic Complexes as Catalysts in the Epoxidation of Cyclohexene. *J. Mol. Catal. A: Chem.* **2003**, 195, 83–94.

9 Miller, M. M.; Sherrington. D. C. Alkene Epoxidations Catalyzed by Mo(VI) Supported on Imidazole-Containing Polymers: II. Recycling of Polybenzimidazole-Supported Mo(VI) in the Epoxidation of Cyclohexene. *J. Catal.* **1995**, 152, 377–383.

10 Bruno, S. M.; Fernandes, J. A.; Martins, L. S.; Gonçalves, I. S.; Pillinger, M.; Ribeiro-Claro, P.; Rocha J.; Valente, A. A. Dioxomolybdenum (VI) Modified Mesoporous Materials for the Catalytic Epoxidation of Olefins. *Catal. Today*, **2006**, 114, 263–271.

11 Handzlik, J.; Ogonowski, J.; Stoch, J.; Mikołajczyk, M. Comparison of Metathesis Activity of Catalysts Prepared by Anchoring of $MoO(acac)_2$ on Various Supports. *Catal. Lett.* **2005**, 101, 65–69.

12 Barlan, A. U.; Basak A.; Yamamoto, H. Enantioselective Oxidation of Olefins Catalyzed by a Chiral Bishydroxamic Acid Complex of Molybdenum. *Angew. Chemie Int. Ed.* **2006**, 45, 5849–5852.

13 Chahboun, G.; Brito, J. A.; Royo, B.; El Amrani, M. A.; Gómez-Bengoa, E.; Mosquera, M. E. G.; T. Cuenca T.; Royo, E. Olefin Epoxidation Catalyzed by *cis*-Dioxdomolybdenum (VI) Complexes Containing Chiral Alkoxo-Imino Ligands Derived from (+)-α-Pinene. *Eur. J. Inorg. Chem.* **2012**, 2940–2949.

14 Gehrke Jr. H.; Veal, J. Acetylacetonate Complexes of Molybdenum (V) and Molybdenum (VI). I. *Inorg. Chim. Acta*, **1969**, 3, 623–627.

15 Soptrajanov, B.; Nikolovski A.; Petrov, I. Infra-Red Spectra of Dioxobis (acetylacetonato) Tungsten (VI) and Dioxobis (acetylacetonato) Molybdenum (VI). *Spectrochim. Acta*, **1968**, 24A, 1617–1621.

16 Topich J.; Bachert III, J. O. Solution IR Spectroscopic Studies of cis-Dioxomolybdenum (VI) Complexes. *Inorg. Chem.* **1992**, 31, 511–515.

17 Craven, B. M.; Ramey E. C.; Wise, W. B. Lability and Stereochemistry of Dioxobis (2, 4-pentanedionato) Molybdenum (VI). *Inorg. Chem.* **1971**, 10, 2626–2628.

18 Judmaier, M. E.; Holzer, C.; VolpeM.; Mösch-Zanetti, N. C. Molybdenum (VI) Dioxo Complexes Employing Schiff Base Ligands with an Intramolecular Donor for Highly Selective Olefin Epoxidation. *Inorg. Chem.* **2012**, 51, 9956−9966.

19 Chi Y.; Chou, P.-T. Transition-metal Phosphors with Cyclometalating Ligands: Fundamentals and Applications. *Chem. Soc. Rev.* **2010**, 39, 638–655.

20 Cazaux I.; Cazé, C. Polymer-supported Molybdenum Acetylacetonate. *Eur. Polym. J.* **1993**, 29, 1615–1619.

21 Miller, M. M.; Sherrington D. C.; Simpson, S. Alkene Epoxidations Catalysed by Molybdenum (VI) Supported on Imidazole-Containing Polymers. Part 3. Epoxidation of Oct-1-ene and Propene. *J. Chem. Soc., Perkin Trans. 2*, **1994**, 2091–2096.

22 Gil, S.; Gonzalez, R.; Mestres, R.; Sanz V.; Zapater, A. Alkene Epoxidations Catalysed by Mo (VI) Supported on Merrifield's Polymer. *React. Funct. Polym.* **1999**, 42, 65–72.

23 Holm, R. H. Metal-Centered Oxygen Atom Transfer Reactions. *Chem. Rev.* **1987**, 87, 1401–1449.

24 Williams, D. B. G.; Lawton, M. Drying of Organic Solvents: Quantitative Evaluation of the Efficiency of Several Desiccants. *J. Org. Chem.* **2010**, 75,8351-8354.

25 Marshall, I.; Higinbotham, J.; Bruce S.; Freise, A. Use of Voigt Lineshape for Quantification of in Vivo ^{1}H Spectra. *Magn. Reson. Med.* **1997**, 37, 651–657.

26 Howarth, D. F.; Weil J. A.; Zimpel, Z. Generalization of the Lineshape Useful in Magnetic Resonance Spectroscopy. *J. Magn. Reson.* **2003**, 161, 215–221.

27 Schmidt, M. W.; Baldridge, K. K.; Boatz, J. A.; Elbert, S. T.; Gordon, M. S.; Jensen, J. H.; Koseki, S.; Matsunaga, N.; Nguyen, K. A.; Su, S. J.; Windus, T. L.; Dupuis M.; Montgomery, J. A. General Atomic and Molecular Electronic Structure System. *J. Comput. Chem.* **1993**, 14, 1347–1363.

28 Couty M.; Hall, M. B. Basis Sets for Transition Metals: Optimized Outer p Functions. *J. Comput. Chem.* **1996**, 17, 1359–1370.

29 Yang, Y.; Weaver M. N.; Merz, Jr., K. M. Assessment of the "6-31+G** + LANL2DZ" Mixed Basis Set Coupled with Density Functional Theory Methods and the Effective Core Potential: Prediction of Heats of Formation and Ionization Potentials for First-Row-Transition-Metal Complexes. *J. Phys. Chem. A*, **2009**, 113, 9843–9851.

30 Stephens, P.; Devlin, F.; Chabalowski C.; Frisch, M. J.; *Ab Initio* Calculation of Vibrational Absorption and Circular Dichroism Spectra Using Density Functional Force Fields. *J. Phys. Chem.* **1993**, 98, 11623–11627.

31 Peverati R.; Truhlar, D. G. A Global Hybrid Generalized Gradient Approximation to the Exchange-Correlation Functional that Satisfies the Second-Order Density-Gradient Constraint and has Broad Applicability in Chemistry. *J. Chem. Phys.* **2011**, 135, 191102.

32 Gräfenstein, J.; Izotov D.; Cremer, D. Avoiding Singularity Problems Associated with meta-GGA (generalized gradient approximation) Exchange and Correlation Functionals Containing the Kinetic Energy Density. *J. Chem. Phys.* **2007**, 127, 214103.

33 Wheeler, S. E.; Houk, K. N. Integration Grid Errors for meta-GGA-predicted Reaction Energies: Origin of Grid Errors for the M06 Suite of Functionals. *J. Chem. Theory Comput.* **2010**, 6, 395–404.

34 Yu, H. S.; Truhlar, D. G.; Database of Frequency Scale Factors for Electronic Model Chemistries - version 3beta3, University of Minnesota, https://t1.chem.umn.edu/freqscale/index.html (accessed July 2016).

35 NIST Computational Chemistry Comparison and Benchmark Database, NIST Standard Reference Database Number 101 Release 16a, 2013, Editor: R. D. Johnson III, http://cccbdb.nist.gov/ (accessed July 2016).

36 Marenich, A. V.; Cramer C. J.; Truhlar, D. G. Universal Solvation Model Based on Solute Electron Density and on a Continuum Model of the Solvent Defined by the Bulk Dielectric Constant and Atomic Surface Tensions. *J. Phys. Chem. B.* **2009**, 113, 6378–6396.

37 Ditchfield, R. Self-Consistent Perturbation Theory of Diamagnetism: I. A Gauge-Invariant LCAO Method for NMR Chemical Shifts. *Mol. Phys.* **1974**, 27, 789–807.

38 Freitag, M. A.; Hillman, B.; Agrawal A.; Gordon, M. S. Predicting Shielding Constants in Solution Using Gauge Invariant Atomic Orbital Theory and The Effective Fragment Potential Method. *J. Chem. Phys.* **2004**, 120, 1197–1202.

39 Hippler M.; Hertz, H. G. Z. Nuclear Magnetic Resonance Study of Proton Relaxation in Liquid Formamide, and of its Intermolecular Structure. *Z. Physik. Chem.* **1992**, 175, 25-39.

40 Hippler, M. Proton Relaxation and Intermolecular Structure of Liquid Formic Acid: a Nuclear Magnetic Resonance Study. *Phys. Chem. Chem. Phys.* **2002**, 4, 1457–1463.

41 Hall, C. D. Sharpe, N. W. Variable-temperature NMR Investigation into the Fluxional Thermodynamics of Metallocene-containing Cryptands. *Organometallics*, **1990**, 9, 952–959.

42 Gutowsky H. S. Cheng, H. N. Determination of Kinetic Parameters by the Frequency Dependence of the NMR Coalescence Temperature. *J. Chem. Phys.* **1975**, 63, 2439–2441.

43 Talsi, E. P.; Klimov O. V.; Zamaraev, K. I. Characterization with ^{95}Mo, ^{17}O, ^{1}H NMR and EPR of Alkylperoxo, Alkoxo, Peroxo and Diolo Molybdenum (VI) Complexes Formed in the Course of Catalytic Epoxidation of Cyclohexene with Organic Hydroperoxides. *J. Mol. Catal.* **1993**, 83, 329–346.

44 Carmona, D.; Ferrer, J.; Pilar Lamata, M.; Oro, L. A.; Limbach, H.-H.; Scherer, G.; Elguero J.; Jimeno, M. L. Determination of the Free Activation Energy for the Breaking of the ^{31}P $^{107(109)}$Ag Bond in [(η^6-p-cymene)Ru(μ-pz)$_3$Ag(PPh_3)]. *J. Organomet. Chem.* **1994**, 470, 211–214.

45 Desponds O.; Schlosser, M. The Activation Barrier to Axial Torsion in 2,2′-bis(diphenylphosphino)biphenyl. *Tetrahedron Lett.* **1996**, 37, 47–48.

46 Akke, M. NMR Methods for Characterizing Microsecond to Millisecond Dynamics in Recognition and Catalysis. *Curr. Opin. Struct. Biol.* **2002**, 12, 642–647.

47 Fielding, L. NMR Methods for the Determination of Protein–Ligand Dissociation Constants. *Prog. Nucl. Mag. Res. Sp.* **2007**, 51, 219–242.

48 Gore E. S.; Gutowsky, H. S.; Chemical Exchange and Transient Effects in an AB-Type NMR Spectrum. *J. Chem. Phys.* **1968**, 48, 3260–3267.

49 Shortridge, M. D.; Hage, D. S.; Harbison G. S.; Powers, R. Estimating Protein−Ligand Binding Affinity Using High-Throughput Screening by NMR *J. Comb. Chem.* **2008**, 10, 948–958.

50 Akitt J. W.; Mann B. E. *NMR and Chemistry: an Introduction to Modern NMR Spectroscopy*, 4th Edition, Nelson Thornes Ltd, 2000, Cheltenham, p189.

51 Selenko, P.; Serber, Z.;.Gadea, B; Ruderman J.; Wagner, G. Quantitative NMR Analysis of the [rotein G B1 Domain in Xenopus Laevis Egg Extracts and Intact Oocytes. *P. Natl. Acad. Sci. USA*, **2006**, 103, 11904–11909.

52 Benco, L.; Bucko T.; Hafner, J. Dehydrogenation of Propane over Zn MOR. Static and Dynamic Reaction Energy Diagram. *J. Catal.* **2011**, 277, 104–116.

53 Bowie, J. H.; Cameron, D. W.; Schütz P. E.; Williams, D. H. Solvent Effects in NMR Spectroscopy—VI: Chemical Shifts Induced by Benzene in Quinones. *Tetrahedron*, **1966**, 22, 1771–1775.

54 Gavriluta, A.; Büchel, G. E.; Freitag, L.; Novitchi, G.; Tommasino, J. B.; Jeanneau, E.; Kuhn, P.-S.; González, L.; Arion V. B.; Luneau, D. Mechanism Elucidation of the *cis–trans*

Isomerization of an Azole Ruthenium–Nitrosyl Complex and its Osmium Counterpart. *Inorg. Chem.* **2013**, 52, 6260−6272.

55 Cooper J.; Ziegler, T. A Density Functional Study of SN2 Substitution at Square-Planar Platinum (II) Complexes. *Inorg. Chem.* **2002**, 41, 6614−6622.

56 Gonzalez C.; Schlegel, H. B. Reaction Path Following in Mass-Weighted Internal Coordinates. *J. Phys. Chem.* **1990**, 94, 5523–5527.

57 Politzer, P.; Toro-Labbé, A.; Gutiérrez-Oliva, S.; Herrera, B.; Jaque, P.; Concha M. C.; Murray, J. S. The Reaction Force: Three Key Points Along an Intrinsic Reaction Coordinate. *J. Chem. Sci.* **2005**, 117, 467–472.

58 Ray P.; Dutt, N. Kinetics and Mechanism of Racemization of Optically Active Cobaltic Trisbiguanide Complex. *J. Indian Chem. Soc.* **1943**, 20, 81– 92.

59 Bailar, J.C. Some Problems in the Stereochemistry of Coordination Compounds: Introductory Lecture. *J. Inorg. Nucl. Chem.* **1958**, 8, 165–175.

60 Rodger A.; Johnson, B. F. G. Which is More Likely: the Ray-Dutt Twist or the Bailar Twist? *Inorg. Chem.* **1988**, 27, 3061–3062.

Graphical Abstract